Analyzing power for ^{4}He($\vec{n}$, n)^{4}He elastic scattering at 50.4 MeV

R. L. York,* J. C. Hiebert, H. L. Woolverton,† and L. C. Northcliffe

Cyclotron Institute, Texas A&M University, College Station, Texas 77843

(Received 10 September 1982)

The analyzing power $A_y(\theta)$ for elastic scattering of neutrons by ^{4}He has been measured for eight angles in the range $80° < \theta_{\text{lab}} < 150°$ at 50.4 MeV. A polarized neutron beam ($p_n = 0.50$) was produced through bombardment of a high-pressure deuterium target by a 50 MeV polarized deuteron beam ($p_d = 0.55$) and by collimation of the neutrons in the 0° direction. A liquid-helium polarimeter placed in the neutron beam was used to measure asymmetries for left and right elastic scattering, with cyclic beam polarization reversal. Multiparameter methods of data acquisition and analysis were used to discriminate against backgrounds from ^{4}He breakup reactions and from interactions with the target-cell walls. The extracted A_y values exhibit the large positive maximum at backward angles and the smaller negative minimum at more forward angles typical of n-^{4}He scattering at lower energies. The n-^{4}He A_y values are compared with p-^{4}He results at a nearby energy by means of a phase-shift analysis and are found to be in good agreement (except perhaps in the negative minimum) when Coulomb corrections to the phase shifts are taken into account.

$$\left[\text{NUCLEAR REACTIONS } {}^4\text{He}(\vec{n},n){}^4\text{He}, E_n = 50.4 \text{ MeV; measured } A_y \right.$$
$$\left. \text{vs } \theta \text{ for } 80° < \theta_{\text{lab}} < 150°. \right]$$

I. INTRODUCTION

The study of the analyzing power $A_y(\theta)$ for n-^{4}He elastic scattering has long been of interest from both practical and theoretical viewpoints. Theoretically, the scattering of spin-$\frac{1}{2}$ particles from a spin-0 target is the simplest process yielding insight into the spin-dependent part of the nuclear interaction, and a comparison of p-^{4}He and n-^{4}He scattering provides a test of our ability to separate Coulomb from nuclear effects and leads to a test of the validity of the charge symmetry hypothesis for nuclear forces. Practically, the fact that n-^{4}He elastic scattering has a large analyzing power at certain angles and the fact that helium scintillates make this reaction attractive as the basis for construction of a neutron polarimeter, and measurements of $A_y(\theta)$ are important for its calibration.

In the past twenty years or so, extensive n-^{4}He analyzing power measurements have been made at numerous energies below 20 MeV, but the analyzing power values used in practice usually have been calculated with phase shifts derived from limited n-^{4}He cross section and polarization data, or inferred from the more accurately determined p-^{4}He phases by invoking charge symmetry principles.[1−5] In the 20—30 MeV energy region, Broste *et al.*[6] and Lisowski *et al.*[7] have measured $A_y(\theta)$ for n-^{4}He scattering, and the comparison by Lisowski *et al.*[7]

showed reasonable agreement between p-^{4}He and n-^{4}He data. The only data above 30 MeV are a limited set of asymmetries measured at 34.1 MeV.[8] The absence of neutron analyzing power data above 30 MeV has been a severe handicap in experiments aimed at determining final state polarizations and polarization transfer parameters at these higher energies.

This paper reports measurements of n-^{4}He analyzing power values at 50.4 MeV, and when considered in combination with the recently published p-^{4}He $A_y(\theta)$ data of Imai *et al.*[9] at nearly the same energy, provides the first opportunity for a quantitative comparison of n-^{4}He and p-^{4}He analyzing power values at energies above 30 MeV. The comparison is made using p-^{4}He analyzing power values based on phase shift fits to the p-^{4}He data interpolated to a center-of-mass energy equivalent to that of this experiment.

II. EXPERIMENTAL DETAILS

The experiment was performed at the neutron facility of the Texas A&M variable energy cyclotron using the ^{2}H($\vec{d}$, $\vec{n}$)^{3}He reaction as a source of polarized neutrons and a liquid-helium polarimeter to measure the asymmetry in the scattering of these neutrons. Since a description of that facility has

been published,[10] only a fragmentary description will be given here.

A. Polarized deuteron beam

An atomic-beam-type polarized ion source was used to provide a vector polarized deuteron beam which was injected axially into the cyclotron and then accelerated.[11] The source nominally produced beam intensities of 15 μA which resulted in a 200 nA beam on target at 50 MeV. The beam polarization was continuously monitored upstream of the experiment in a polarimeter utilizing d-^{4}He elastic scattering at $\theta_{lab}=70°$. While the d-^{4}He analyzing power has been measured for deuteron energies up to 45 MeV,[12] it was not known at higher energies. Thus a measurement of A_y at 70° laboratory was necessary to calibrate the polarimeter.

This measurement was made by first determining the beam polarization at 45 MeV where the d-^{4}He analyzing power is known,[12] then retuning the cyclotron to extract a 50.5 MeV beam, in a time short compared with that of any observed variation of the beam polarization, and finally remeasuring the asymmetry in the polarimeter, from which A_y was determined. The value obtained for the d-^{4}He analyzing power at 50.5 MeV was $A_y(70°)=0.57\pm0.03$.

B. Polarized neutron beam

A high pressure deuterium gas cell was used as the neutron production target, yielding neutrons from the ^{2}H$(\vec{d},\vec{n})^3$He reaction.[13] The high-density liquid-nitrogen-cooled gas target was necessary because of the relatively small cross section, 39 mb/sr, at 50 MeV. The target had an areal density of 1.84×10^{22} atoms/cm^2. The 0° neutron beam intensity, 4.5 m from the production target, was 2.2×10^3 neutrons/cm^2 per 100 nA of deuteron beam. The energy loss of the deuteron beam in the target gas was 1.33 MeV and this loss was reflected in the energy spread of the neutron beam. After the deuteron beam passed through the target, it was magnetically deflected through 90° and stopped in a beam-dump Faraday cup. The Faraday cup was buried in approximately one cubic meter of steel surrounded by iron-enriched concrete so as to shield the neutron polarimeter from the high background radiation produced in the stopping of the beam.

The liquid-helium polarimeter,[10,14] which served as a neutron detector, was located 4.5 m from the neutron-production target and was shielded from the target by a 2.12 m wall of concrete blocks. The neutrons emerging from the production target at 0° were collimated with two steel cylinders of length 60.9 cm, placed at the entrance and exit of a channel

through the shield wall. These cylinders contained tapered steel inserts which formed a 2.5 cm square aperture at the exit of the collimator. The profile of the neutron beam at the location of the polarimeter target cell was studied and found to be satisfactory.[10]

The polarization of neutrons produced in the ^{2}H$(\vec{d},\vec{n})^3$He reaction at 0° is expected to be equal to the polarization of the neutrons within the incident polarized deuteron beam. Simmons et al.[15] first proposed that the vector polarization transfer coefficient $K_y^{y'}(0°)$ could be predicted by calculating the spin polarization of the neutrons within a polarized deuteron beam and assuming that this polarization is retained by the neutrons after the reaction. If a 6% D-state component in the deuteron wave function is assumed, the calculated value[16] for pure vector polarized deuterons is $K_y^{y'}(0°)=0.607$. A refined calculation[17] which incorporates results obtained with both vector and tensor polarized deuteron beams yields $K_y^{y'}(0°)=0.615$. Evidence that the simple stripping model used to calculate $K_y^{y'}(0°)$ is valid at higher energies has been presented,[16] and in particular comes from a measurement[18] of the charge symmetric reaction ^{2}H$(\vec{d},\vec{p})T$ at 50.6 MeV. The value obtained was $K_y^{y'}(0°)=0.62\pm0.03$, in excellent agreement with the calculated value. With the typical value, $P_d=0.55$, for vector polarization of the deuteron beams available from the cyclotron, the neutron beam polarization expected is

$$P=\tfrac{3}{2}P_dK_y^{y'}=0.507 . \tag{1}$$

In all runs of the present experiment the neutron beam polarization as given by Eq. (1), with $K_y^{y'}=0.615$, was 0.50 and stayed constant within ±0.005, although the normalization uncertainty was no better than 0.03.

C. Liquid-helium polarimeter

Because many neutron polarization experiments have been performed at lower energies, several polarimeters have been built elsewhere, most of which used high-pressure helium as the polarization analyzer. Elastic n-^{4}He scattering is usually used as the analyzing reaction because of its large analyzing power at certain angles, and because the recoiling He ions cause scintillations in the helium. Not only do these scintillators provide information about the helium recoil energy and the neutron time-of-flight, but also the requirement that they be in coincidence with a signal from a scattered neutron detector helps in discrimination against backgrounds.

At 50 MeV there are several advantages to the use of a liquid-helium target rather than one of high-pressure helium gas. A liquid-helium target is 5.5

times more dense than a typical high-pressure gas target. Not only does this greatly increase the detection efficiency, but it also substantially reduces the edge effects arising from finite target size, since the range of the recoiling helium ions is a factor of 6 smaller in the liquid target than in a typical high-pressure gas target. In addition, with the latter it is necessary to add a second gas such as krypton or xenon to obtain adequate scintillation intensity. Scattering from this "background" gas affects the measured asymmetries and the corrections for this effect are often difficult to evaluate.[3] With liquid helium this problem is avoided since the scintillation intensity from the helium itself is adequate and additives are not needed, although the scintillation photons have wavelengths in the ultraviolet region and the walls of the target cell must be coated with a wavelength shifter to convert the wavelengths into a spectral region where photomultiplier tubes are sensitive.[19]

The liquid-helium polarimeter used in this experiment is similar in design to the polarimeter of Simmons and Perkins,[20] except that the scattering plane is horizontal rather than vertical. Basically the polarimeter[10,21] consists of a liquid-helium target cell surrounded by four scattered-neutron detectors placed in symmetric left/right pairs at two scattering angles. The detectors are rectangular blocks of Ne102 scintillator of width 5.1 cm, height 20.3 cm, and thickness 7.6 cm located 40.6 cm (center to center) from the He target. The He scintillations are detected by a photomultiplier tube which views the target from below through a sapphire window.

The requirement of a coincidence between signals from the liquid-helium cell and one of the four NE102 scattered neutron detectors defines the neutron scattering angle. A plot of neutron time-of-flight t from the neutron production target to the helium cell versus helium pulse height H ideally should contain only the kinematic loci for neutrons scattered elastically at the fixed detector angles. In practice, however, there is considerable background in the spectra and good pulse-height resolution is necessary to separate the kinematic loci cleanly from the background.

Although this liquid-helium polarimeter has been used successfully in earlier experiments,[22–24] a recurrent problem has been that of consistently obtaining good helium pulse-height resolution. The most important factor affecting the resolution in H is the light-collection efficiency of the target cell system. This efficiency depends on several factors in the target design. These include: (1) the purity of the liquid helium, (2) the reflectivity of the ceramic cup which defines the target volume, (3) the effectiveness of the wavelength shifter, (4) the transmission prop-
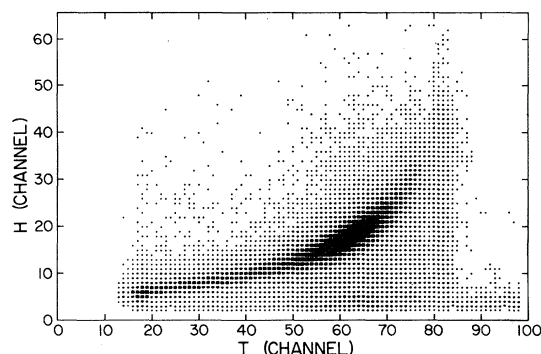

FIG. 1. A neutron time-of-flight vs liquid-helium pulse-height spectrum with good pulse-height resolution. The kinematic locus of the elastically scattered neutrons is well defined in this spectrum.

erties of the sapphire window which forms the bottom of the helium cell, (5) the efficiency of the light pipe, and (6) the quality of the photomultiplier tube. While the effects of all of these factors were investigated, the one that proved to be the cause of the unpredictable resolution was contamination of the liquid helium. At liquid-helium temperature, contaminant gases such as air would form a frostlike material, which settled to the bottom of the cryostat and collected on the sapphire window, diminishing the light transmission through the window, and hence the overall light collection efficiency. Identification of this as the source of the occasional poor H resolution was difficult because the frost would disappear whenever the cryostat warmed up. When measures were taken to ensure that only "clean"
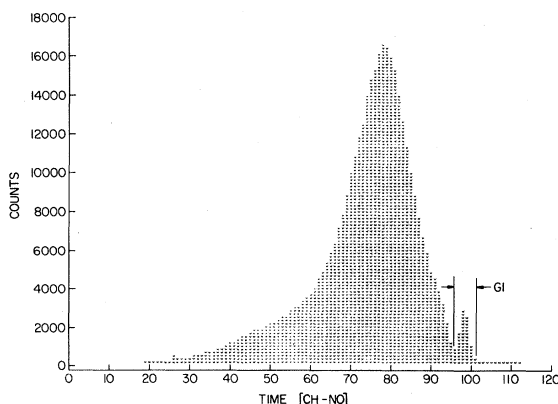

FIG. 2. A neutron time-of-flight spectrum. The small peak at channel 98 corresponds to the monoenergetic neutrons from the $^2H(d,n)^3He$ reaction. The continuum at lower t values corresponds to the $^2H(d,n)$ breakup reactions.

liquid helium was transferred to the cryostat and that a positive helium pressure was maintained in the cryostat at all times, good H resolution was obtained consistently.

Although improvements to other parts of the system were made, the study of H resolution was not systematic enough to determine the effects of each of the parameters involved, but the net result was that the combination of these improvements yielded considerably better liquid-helium pulse-height resolution. Tests using an ^{241}Am alpha source inside the liquid-helium cell yielded a resolution of 12% FWHM, while similar measurements by Broste et al.[6] and Lam et al.[25] gave resolutions of 17% and 30%, respectively. The resolution for helium recoils from n-^{4}He elastic scattering at 50 MeV averaged about 13% FWHM. An example of the kinematic locus obtained with this resolution is shown in Fig. 1.

D. Scattering measurements

Four parameters associated with each scattering event were written directly onto magnetic tape for later analysis. In addition to t and H, already defined, these parameters included δt, the time-of-flight (TOF) from the helium cell to the scattered neutron detector, and P, the pulse height from the scattered neutron detector. A tag word was also recorded with each event to identify which of the four scintillators detected the scattered neutron. In order to ensure that only elastically scattered neutrons were used in determination of the $\vec{n}$-^{4}He scattering asymmetries, it was necessary to reconstruct individual events and study correlations among the various parameters.

The neutron TOF parameter t was generated using a time-to-amplitude converter, which was started by a pulse from the helium-cell photomultiplier tube in coincidence with a pulse from one of the four scattered-neutron detectors and stopped by a pulse from a discriminator triggered by the cyclotron radiofrequency (rf) waveform. Since the cyclotron produces a beam with a repetitive micropulse time structure, there is ideally a fixed phase relationship between the rf dee voltage and a beam pulse striking the neutron production target. The neutron TOF resolution depends partly on the stability of this phase relationship and partly on the inherent time width of the beam micropulses. In order to resolve the monoenergetic neutron group corresponding to the ^{2}H($\vec{d}$,$\vec{n}$)^{3}He reaction from the continuum of breakup neutrons with the 4.5 m flight path used, it was necessary to have beam micropulses of time width no greater than ~2.5 ns. Since the 50 MeV deuteron beams produced by the cyclo-
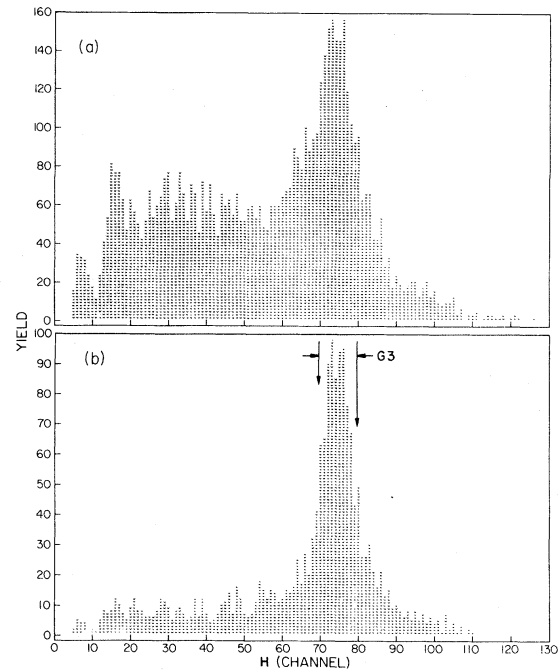

FIG. 3. Helium recoil pulse-height distributions: (a) subject only to a t gate selecting events induced by 50 MeV neutrons, and (b) subject also to the δt gate shown in Fig. 4(a).

tron typically have micropulse widths of ~6 ns, it was necessary to "time tune" the cyclotron, that is, to narrow this width by empirical adjustment of the currents in the trim and valley coils of the accelerator. A typical neutron TOF spectrum obtained using this technique is shown in Fig. 2. The small peak at the high end of the spectrum is produced by the ^{2}H($\vec{d}$,$\vec{n}$)^{3}He neutrons. The much larger and broader peak is associated with neutrons from ^{2}H($\vec{d}$,$\vec{n}$) breakup reactions.

E. Analysis

When the data tapes were replayed in the off-line analysis, two-dimensional arrays of all possible combinations of the four recorded parameters could be constructed. Further, a variety of gating modes could be used to examine correlations between any two parameters in terms of the others. For this experiment, a gate (G1) was set on the t spectrum to limit the analysis to events associated with the ^{2}H(d,n)^{3}H neutrons; in the remaining discussion, only those events will be considered.

As noted earlier, the coincidence requirement defines the scattering angle of the neutron, and thus determines the division of energy between the scattered neutron and the recoil helium ion. For elastic scattering the helium recoil spectrum should exhibit a well-defined peak of width which reflects the
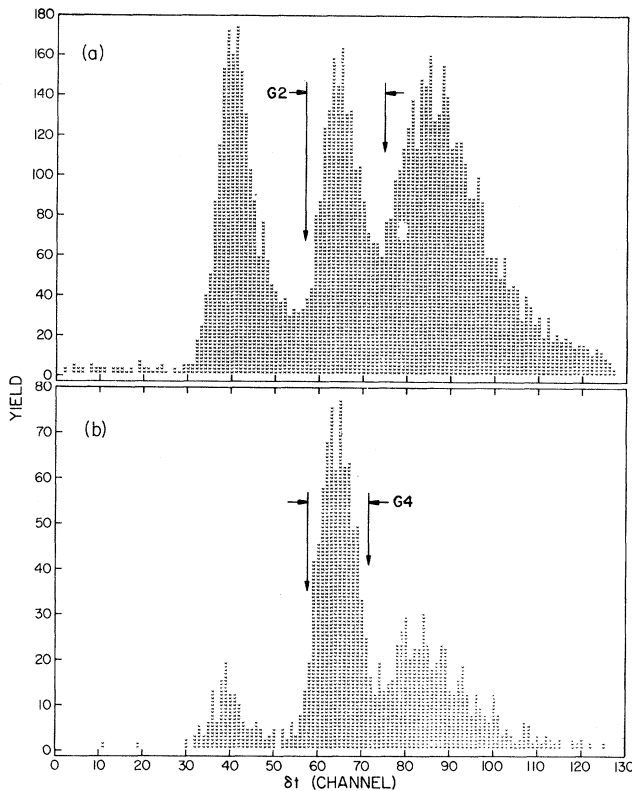
FIG. 4. (a) A δt spectrum for 50 MeV neutrons scattered at $\theta_{lab} = 120°$. From left to right the peaks correspond to detected gamma rays, n-^{4}He elastic scattering, and n-^{4}He inelastic scattering. (b) The same δt data subjected to a gate on the helium pulse height as shown in Fig. 3(b). Contributions from gamma rays and inelastically scattered neutrons are still evident.

pulse-height resolution of the liquid-helium detector. A typical H spectrum is shown in Fig. 3(a). It is obvious from this spectrum that the recoil helium peak is not cleanly resolved and its width is much larger than the intrinsic resolution of the detector (12%).

From run to run, small gain shifts were seen in the H spectra. These were caused by counting rate differences, and were largest for the empty-target runs. These shifts were removed in the analysis by rescaling the H value for each event of a run to compensate for the gain shift observed in that run.

The reason for the poor resolution seen in Fig. 3(a) can be determined by examining the δt spectrum, which is shown in Fig. 4(a). If the only process taking place was elastic n-^{4}He scattering of the ^{2}H$(d,n)^3$He neutrons, a single sharp peak would be expected, and in fact, the central peak in the spectrum corresponds to such n-^{4}He elastic scattering. The events to the left of this peak have a shorter δt and are produced by gamma rays which come primarily from interactions of the beam with the walls

of the helium cell. The events to the right of the elastic peak have larger δt and correspond to scattered neutrons of lower energy. A two-dimensional plot of δt vs H shows that events in the elastic peak are associated with well-defined values of H. The events corresponding to larger δt have a roughly random distribution in H. Since all of these events are initiated by neutrons of the same energy, the events with larger δt than the elastic events must be produced by inelastically scattered neutrons. Inelastic reactions can occur because 50 MeV incident neutrons are well above the breakup threshold of ^{4}He, and such breakup can produce a wide range of H values.

When the H values are restricted to those of elastic neutrons by imposing the δt gate ($G2$) indicated in Fig. 4(a), the H resolution is much improved [Fig. 3(b)]. The width of the elastic peak becomes consistent with the intrinsic resolution measurements made with the alpha source. Although this resolution is better than that obtained in n-^{4}He experiments at lower energy,[6,21] it is still not adequate to ensure that only elastic neutrons are included in the asymmetry determinations. When a δt spectrum is generated using the narrow gate ($G3$) on H indicated in Fig. 3(b), contributions from reactions other than elastic scattering are still evident [Fig. 4(b)]. This spectrum shows that inelastic neutrons or n-^{4}He scattering events coincident with a gamma ray in an NE102 detector can yield values of H equal to those of elastic n-^{4}He events. Therefore, the additional gate ($G4$) shown in Fig. 4(b) was also imposed on the data. Only those events which fell within the separate gates $G1$, $G3$, and $G4$ on t, H, and δt, respectively, were used in the determination of the asymmetries. The great importance of using multiparameter data acquisition and analysis methods should be evident from this discussion.

The yield for the scattering of polarized neutrons from a spin-0 target is given by

$$I(\theta) = I_0(\theta)[1 + \vec{P} \cdot \hat{n} A(\theta)], \qquad (2)$$

where $\vec{P}$ is the incident neutron polarization, $\hat{n}$ is the unit vector normal to the scattering plane in the direction of $\vec{k}_{in} \times \vec{k}_{out}$, and $A(\theta)$ is the analyzing power of the reaction. In the present experiment all scatterings occur nominally in the horizontal plane, so that $\hat{n}$ points "up" for left scatterings and "down" for right scatterings. Similarly, the incident neutron polarization is either up or down, as determined by the deuteron beam orientation produced at the ion source.

The desired scattering asymmetries, $\epsilon(\theta)$, were obtained by collecting elastic scattering yields L^u, L^d, R^u, and R^d, where L/R signifies yields in the left/right detectors and u/d denotes up/down orien-

TABLE I. Neutron asymmetries and analyzing powers in n-^{4}He elastic scattering at 50.4 MeV laboratory energy. The corrections shown in the fourth column are combined corrections for plural scattering and finite geometry.

θ_{lab} (deg)	θ^* (deg)	$\epsilon(\theta^*)$	Correction	$A_y(\theta^*)$
80.0	94.9	0.030±0.026	1.320±0.070	0.08±0.07
95.0	110.0	−0.203±0.038	1.090±0.010	−0.44±0.09
100.0	114.8	−0.171±0.040	1.106±0.007	−0.38±0.09
110.0	124.1	−0.025±0.114	1.413±0.048	−0.07±0.16
120.0	133.0	0.233±0.037	1.056±0.003	0.49±0.08
135.0	145.6	0.427±0.028	1.048±0.001	0.89±0.07
140.0	149.6	0.415±0.026	1.042±0.001	0.86±0.06
150.0	157.4	0.332±0.036	1.031±0.002	0.68±0.08

tations of the incident neutron beam polarization. The polarization of the incident neutrons was cyclically reversed by reversing the magnetic field in the ionizer in the pattern up-down-down-up, in order to minimize errors due to long term changes in the beam polarization, the cyclotron operating conditions, and the data acquisition electronics. False asymmetries due to differences in detector solid angles and efficiencies, and to errors in beam current integration, were minimized by using the ratio method to calculate the asymmetries. In this method the ratio of yields

$$r(\theta) = \left[\frac{L^u R^d}{L^d R^u} \right]^{1/2} \tag{3}$$

is formed, and the experimental asymmetry is obtained directly from $r(\theta)$ by means of the relation

$$\epsilon(\theta) = \frac{r(\theta)-1}{r(\theta)+1} . \tag{4}$$

The measured asymmetries must be corrected for the effects of plural scattering of the neutrons in the helium and for the finite geometry of the polarimeter. The code PMS1,[26] commonly used at lower energies, has been modified[27] to include relativistic kinematics and absorption effects in n-^{4}He scattering. Since the polarimeter detectors subtended 7.2° in the scattering plane and 28.6° in azimuthal angle from the target center, the dominant contribution was due to finite geometry. The largest calculated ratio of plural to single scattering was 0.015 at $\theta = 95°$.

The measured asymmetries are given in Table I, along with the calculated multiplicative correction factors for plural scattering and finite geometry and the final corrected analyzing power values. These corrected $A_y(\theta)$ values are also shown in Fig. 5. The errors shown in Table I and Fig. 5 are statistical only, and do not reflect the overall normalization

uncertainty, which is estimated to be ~5% of the A_y value.

III. PHASE SHIFT ANALYSIS

There are several obstacles to a test of charge symmetry by direct comparison of these n-^{4}He $A_y(\theta)$ values with available p-^{4}He $A_y(\theta)$ values: The experiments were not done at the same energy; it is necessary to take Coulomb effects into account; and allowance must be made for the neutron proton mass difference. One means of handling these prob-
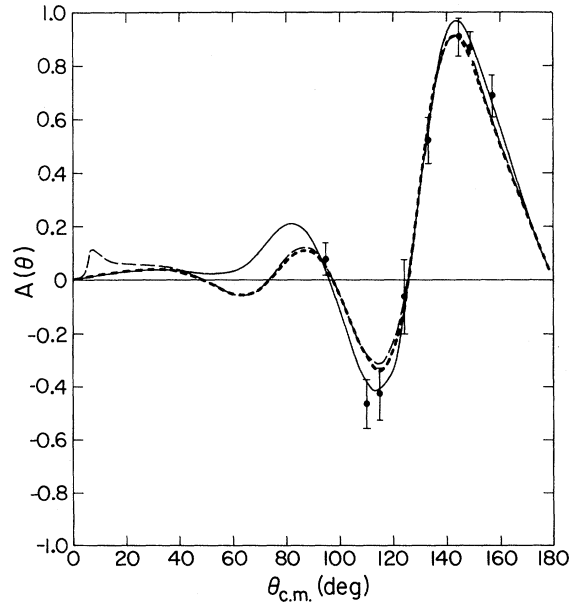

FIG. 5. A comparison of the measured n-^{4}He analyzing powers and the phase-shift calculations. The heavy dashed curve is the fit to the Imai et al. p-^{4}He data for $\theta^* > 40°$, assuming that these are 51.0 MeV n-^{4}He data. The solid curve represents the fit to the present data (see text) and the light dashed curve is a p-^{4}He prediction using phase shifts interpolated to 51.7 MeV.

lems is through the mechanism of a phase-shift analysis.

In order to obtain a set of n-^{4}He phase shifts at 50.4 MeV it is necessary to have a considerably larger data set than is provided by the present experiment. If charge symmetry is assumed, this can be done by using the recent p-^{4}He data of Imai et al.[9] at $E_p = 52.3$ MeV to expand the data base for a n-^{4}He phase shift analysis. According to the prescription of Hoop and Barschall,[3] the neutron and proton data should be compared at center-of-mass energies E^* equally displaced from the energies of the respective mass-5 excited states. For 50.4 MeV neutrons, $E^* = 40.08$ MeV, which is 22.41 MeV above the ^{5}He excited state at 17.67 MeV. Since the mirror state in ^{5}Li is at 18.73 MeV, the corresponding center-of-mass energy for the p-^{4}He system is 41.14 MeV. This requires a proton laboratory energy of 51.7 MeV. The 52.3 MeV data[9] are the nearest and the most complete p-^{4}He data set available.

A phase shift program has been written[27] which calculates nucleon-^{4}He scattering using relativistic kinematics and includes partial waves up to H waves. The fitting part of the code follows the procedures of the program CURFIT (Ref. 28) and includes the option of multiple passes during which only selected phase shifts and/or absorption parameters are varied. Searches are performed by minimizing the quantity X^2 defined as

$$X^2 = \sum_{i=1}^{N_1} \left[\frac{\sigma_{\text{th}}(\theta_i^*) - \sigma_{\text{ex}}(\theta_i^*)}{\Delta\sigma(\theta_i^*)} \right]^2$$
$$+ \sum_{i=1}^{N_2} \left[\frac{A_{\text{th}}(\theta_i^*) - A_{\text{ex}}(\theta_i^*)}{\Delta A(\theta_i^\theta)} \right]^2 , \qquad (5)$$

where $\sigma_{\text{th}}(\theta_i^*)$ and $\sigma_{\text{ex}}(\theta_i^*)$ are the calculated and measured differential cross sections at a set of N_1 center-of-mass scattering angles θ_i^*, A_{th} and A_{ex} are the corresponding analyzing powers at another set of N_2 angles, and $\Delta\sigma$ and ΔA are the quoted experimental errors. The code can be used to fit cross section data alone, analyzing power data alone, or combined data sets.

Initial checks of this code were made at two energies, $E_p = 39.8$ and 55.0 MeV. At 55 MeV the data fitted include the differential cross section data of Hayakawa et al.[29] and the 54.8 MeV analyzing powers of Boschitz et al.[30] The phase shift solution was comparable to that of Houdayer et al.,[31] who fitted the same data set. At 39.8 MeV the data of Bacher et al.[32] were used and the solution was essentially the same as that of Plattner et al.[33] Since the present phase-shift calculation does not include first-order relativistic corrections to the Coulomb scattering amplitudes, direct comparisons of the
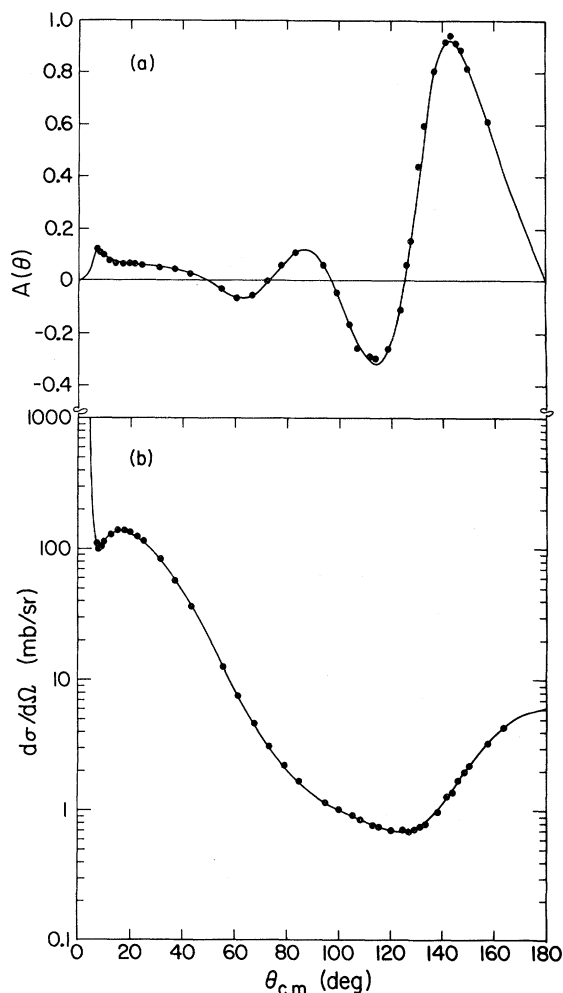

FIG. 6. (a) Differential cross section and (b) analyzing power data of Imai et al. for the elastic scattering of 52.3 MeV protons from ^{4}He. The solid curves represent the results of the present phase-shift analysis.

present p-^{4}He fits with those of the recent analyses[31,33] cannot be made.

A. Fitting of the 52.3 MeV p-^{4}He data

The fit to the high quality data of Imai et al.[9] is shown in Fig. 6. The phase shifts of the Saito[34] solution 2 were used as starting parameters. The typical procedure followed was first to vary the G- and H-wave parameters and then to vary the complete 22 parameter set used in calculating the scattering. The results of the present analysis of the data of Imai et al. can only be compared qualitatively with the complete analysis of these data by Saito.[34] The visual quality of the fit is certainly comparable to that of the Saito fits but detailed comparisons cannot be made until relativistic correc-

TABLE II. Single-energy phase shifts.

| | p-^{4}He at 52.3 MeV[a] | | | | n-^{4}He at 50.4 MeV | | | |
| | Saito (Sol. 2) | | Present | | Imai[b] | | Present data | |
	δ (deg)	η	δ (deg)	η	δ (deg)	η	δ (deg)	η
$S_{1/2}$	60.57	0.648	61.0	0.635	64.7	0.633	64.7	0.633
$P_{3/2}$	60.67	0.892	60.7	0.884	61.2	0.825	61.2	0.825
$P_{1/2}$	27.77	0.975	26.1	1.000	31.9	0.930	27.8	0.930
$D_{5/2}$	26.58	0.517	27.3	0.513	26.0	0.494	27.1	0.494
$D_{3/2}$	14.74	0.616	13.7	0.641	21.6	0.574	21.6	0.574
$F_{7/2}$	14.98	0.930	15.8	0.917	16.2	0.947	16.2	0.947
$F_{5/2}$	7.14	0.933	6.36	0.947	9.41	0.917	9.41	0.917
$G_{9/2}$	3.75	1.000	3.91	0.986	5.42	0.978	5.42	0.978
$G_{7/2}$	0.89	0.937	0.65	0.949	2.27	0.931	2.27	0.931
$H_{11/2}$	0.58	1.000	0.80	0.995	0.91	0.986	0.91	0.986
$H_{9/2}$	0.80	0.994	0.57	0.995	1.34	1.000	1.34	1.000
χ_T^2	0.95		0.99		0.66		0.32	

[a]Data of Ref. 9.
[b]Data of Ref. 9 for $\theta^* > 40°$ analyzed as 51.0 MeV n-^{4}He scattering.

tions[35] are added to the present code. A single attempt to vary the phases obtained in the fit to the 52.3 MeV data (which differ substantially from the interpolation of Houdayer et al.[31]), along with the cross section and analyzing power normalizations, did not improve the fit significantly and has less than a 0.1% effect on the normalizations. This is consistent with the small renormalizations observed in the Saito analysis. The phase-shift solution and the Saito solution 2 are shown in Table II. The quantity χ_T^2 shown in Table II is the usual measure of the quality of the fit, the χ^2 per datum point defined as

$$\chi_T^2 = \chi^2/(N_1 + N_2) .$$

B. 50.4 MeV n-^{4}He analysis

Under the assumption of charge symmetry, the 52.3 MeV proton data should be the same as the 51.0 MeV n-^{4}He data if the comparison is restricted to the angular region in which Coulomb effects are small. As initial input for a phase-shift analysis, the analyzing power values of the present experiment can be supplemented by interpreting the 52.3 MeV proton data of Imai et al.[9] for center-of-mass angles θ^* larger than 40° as 51.0 MeV neutron data. The analyzing power curves given by the resulting phase shifts are compared with the present measurements in Fig. 5 and the differential cross section curves obtained are shown in Fig. 7.

An early phase-shift analysis of the present analyzing power data[21] revealed that the real $P_{1/2}$ and $D_{5/2}$ phase shifts had a strong influence on the

depth of the minimum in $A_y(\theta^*)$ near $\theta^* = 115°$. The analysis was therefore carried one step further by fixing all the parameters except for $\delta(P_{1/2})$ and $\delta(D_{5/2})$ at the 51.0 MeV "neutron values" and then varying these two real phases to minimize χ^2 for the present 50.4 MeV $A_y(\theta^*)$ data set. This fit is shown as a solid line in Fig. 5 and the corresponding n-^{4}He differential cross sections are shown similarly in Fig.
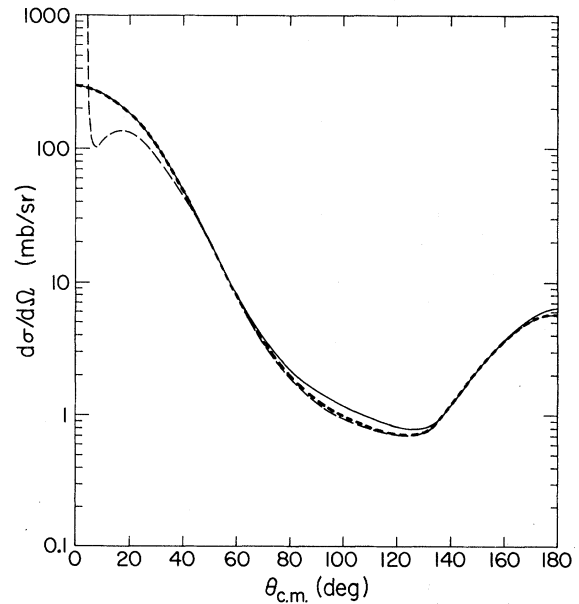

FIG. 7. Phase-shift predictions for the differential cross sections for n-^{4}He and p-^{4}He scattering near 51 MeV. See the caption to Fig. 5 and the text for descriptions of the calculations.

7. The phase-shift solution is given in Table II.

To check the validity of these procedures and test further the prescription being used in comparing n-^{4}He and p-^{4}He scattering, a p-^{4}He prediction was made at 51.3 MeV. This was done by interpolating between the 48.8 MeV phase shifts of Houdayer et al.[31] and the present 52.3 MeV solution. This calculation is shown as a long-dashed line in Figs. 5 and 7. The comparison of the p-^{4}He and n-^{4}He distributions in these two figures provided the basis for the choice of the region $\theta^* > 40°$ for the equivalence between the two reactions.

IV. DISCUSSION

The comparison of the present n-^{4}He $A(\theta^*)$ data with the p-^{4}He data of Imai et al. reveals excellent agreement in the positive peak in the distribution at $\theta^* = 145°$ and a weak discrepancy in the minimum at $\theta^* = 115°$. The lowest n-^{4}He point at 110° is 2.1 standard deviations below the 51.7 MeV proton result, while the second point in the minimum is 0.9 standard deviations below the proton value. These discrepancies are large when compared with the expectations of probability theory. The plural scattering/finite geometry corrections are 9—11% for these two measurements and increase the discrepancy by roughly 10%. Attempts to verify these calculations have been made with a second Monte Carlo code[27] which is simpler in concept but takes vastly more running time. The two codes have produced statistically consistent results in all cases which have been checked. There is only one measured p-^{4}He minimum in the data sets between 45 and 55 MeV which is deeper than -0.35. This occurs in the 48 MeV data of Craddock et al.[36] in which the minimum value is -0.4. The present result of -0.45 ± 0.09 does fall significantly lower than the other p-^{4}He values.[9,30]

It is of interest to use the present results to test recent predictions of n-^{4}He observables obtained by calculating Coulomb corrections to the p-^{4}He phase shifts. These corrections, which are subtracted from the p-^{4}He phase shifts, account for: (i) effects of the extended charge distributions of ^{4}He and the proton and (ii) effects originating in the interference between the Coulomb and strong interactions. Fröhlich et al.[37] have developed a first order approximation relating these Coulomb corrections to the two-body nuclear T matrix in terms of on-shell quantities only. This approximation has been applied to N-N scattering[37] and more recently to n-^{4}He scattering.[38—40] The comparison with R-matrix calculations below 20 MeV demonstrated that these Coulomb corrections account, at least qualitatively, for the differences between n-^{4}He and p-^{4}He data.

The present data provide the first opportunity for testing these calculations above 30 MeV.

Despite the very high quality of the data set of Imai et al.,[9] the energy dependence of the Saito p-^{4}He phase shifts is not particularly smooth. This causes significant uncertainties when an interpolation of the phase shifts to 50.4 MeV is attempted. Since the calculated Coulomb corrections depend on the energy derivatives of the phase shifts, these corrections become even more uncertain. The predictions of Zankel[41] are based on the solution 1 p-^{4}He phase shifts of Saito.[34] Predicted analyzing powers at 50.4 MeV are compared with the present results in Fig. 8. The extremes of the narrow band of predicted n-^{4}He analyzing powers result from two separate interpolations to the p-^{4}He phase shifts. The upper edge of the band in Fig. 8 results when the Coulomb corrections are calculated using p-^{4}He phases fitted between 30 and 52 MeV by second order polynomials. The lower edge of the band results when only the p-^{4}He phases at 45, 52.3, and 59.6 MeV are fitted. The p-^{4}He analyzing power curve obtained by interpolation of the 45—60 MeV Saito phase shifts to 50.4 MeV is also shown in Fig. 8.

The interpolated p-^{4}He prediction at 50.4 MeV reflects the strong energy dependence of $A(\theta^*)$ in the range $65° < \theta^* < 120°$. The minimum at 115° is 13% deeper than the measured value in the 52.3 MeV data set,[9] and thus is in better agreement with the

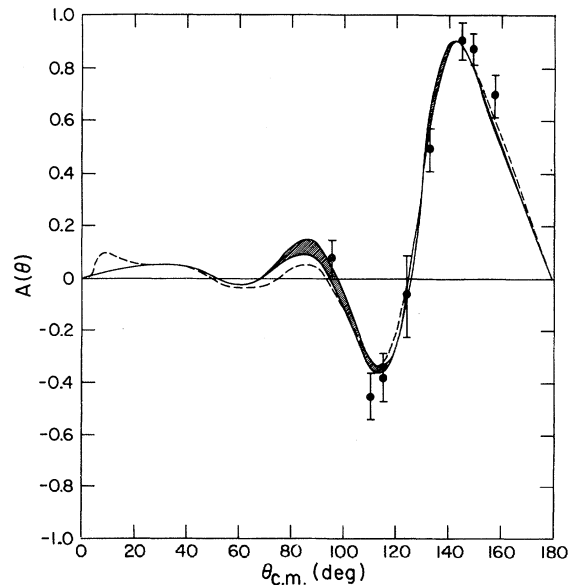FIG. 8. Comparison of charge-symmetric predictions of n-^{4}He analyzing powers at 50.4 MeV (Ref. 41) with the present data. The solid curve and cross-hatched band represent the range of the predictions based on different interpolations to the Saito 1 phase shifts (Ref. 34). The dashed curve is the p-^{4}He prediction at 50.4 MeV.

present measurement. Zankel's calculations[41] have shown that if the Coulomb parameter η, is set to zero and the interpolated p-^{4}He phase shifts are used in a "zero-order" n-^{4}He calculation, the depth of this minimum returns to the 52.3 MeV p-^{4}He value. Inclusion of the calculated Coulomb corrections brings the "full" n-^{4}He prediction back into agreement with the 50.4 MeV p-^{4}He value in the 115° minimum (see Fig. 8). The predicted n-^{4}He analyzing power in the $65° < \theta^* < 120°$ range is seen to be sensitive to the details of the p-^{4}He phase-shift interpolations.

V. CONCLUSION

The agreement between N-^{4}He analyzing powers is excellent for the large back-angle maximum. This is in accord with the Coulomb correction calculations, which predict differences no larger than the order of 1% in the backward maximum. Consequently it is felt that below 60 MeV the p-^{4}He analyzing powers in the region of the backward peak can be used by interpolating the p-^{4}He phase shifts to the properly adjusted center-of-mass energy. The polarization of a neutron beam can be determined by measurements of n-^{4}He asymmetries over the back-angle peak.

Although the present data suggest that there is a small discrepancy between n-^{4}He and p-^{4}He analyzing powers at $\theta^* = 110°$, it is clear that neutron data of higher accuracy will be required in order to determine whether or not this discrepancy is real. It is anticipated that such neutron data will be available shortly from the Karlsruhe cyclotron.[42] These measurements should include the angular range $65° < \theta^* < 90°$ and will thereby tighten constraints on the phase-shift solutions.

The forthcoming n-^{4}He analyzing power data should also help to improve the test of the Coulomb correction predictions. It is also evident that more p-^{4}He data sets of high quality will be required in order to determine fully the energy dependence of the p-^{4}He phase shifts. This is particularly true for the 45 to 52 MeV region in which the analyzing powers for $60° < \theta^* < 110°$ vary dramatically. Since the calculated Coulomb corrections are sensitive to

the energy dependence of the phase shifts, no true test of the theory is possible without additional proton data. These Coulomb corrections must be made before any test of charge symmetry can be addressed *via* N-^{4}He scattering.

In the present analysis the stripping calculation was used to predict the value of $K_y^{y}(0°)$ for the ^{2}H($\vec{d},\vec{n}$)^{3}He reaction. The result, $K_y^{y}(0°) = 0.615$, was used to determine the polarization of the neutron beam and thereby to determine analyzing powers from measured asymmetries. An alternative method which can be used for determination of the polarization of the neutron beam is to set the n-^{4}He analyzing powers in the back-angle maximum of $A_y(\theta^*)$ equal to the p-^{4}He values. If the n-^{4}He analyzing powers at 50.4 MeV are set equal to the p-^{4}He analyzing powers calculated with phase shifts interpolated to 51.7 MeV, then the measured asymmetries at $\theta^* = 145°$ and 150° combined with these inferred analyzing powers determine the neutron polarization through the relation

$$\epsilon(\theta^*) = PA_y(\theta^*) .$$

When this value of P is used in Eq. (1), the measured value for the vector polarization transfer coefficient is

$$K_y^{y'}(0°) = 0.63 + 0.03 .$$

This is consistent with the value 0.62 ± 0.03 obtained[14] for the ^{2}H($\vec{d},\vec{p}$)^{3}H reaction and both are consistent with the theoretical value predicted by the stripping calculation.

---

*Present address: Los Alamos National Laboratory, Los Alamos, NM 87545.

†Present address: Facultät für Physik, Albert Ludwig Universität, Freiburg, Federal Republic of Germany.

[1]J. L. Gammel and R. M. Thaler, Phys. Rev. **109**, 2041 (1958).

[2]D. C. Dodder and J. L. Gammel, Phys. Rev. **86**, 520

(1962).

[3]B. Hoop, Jr. and H. H. Barschall, Nucl. Phys. **83**, 65 (1966).

[4]W. G. Weitkamp and W. Haeberli, Nucl. Phys. **83**, 46 (1966).

[5]Th. Stammbach and R. L. Walter, Nucl. Phys. **A180**, 225 (1972).

[6]W. B. Broste, G. S. Mutchler, J. E. Simmons, R. A. Arndt, and L. D. Roper, Phys. Rev. C 5, 761 (1972).

[7]P. W. Lisowski, R. L. Walter, G. G. Ohlsen, and R. A. Hardekopf, Phys. Rev. Lett. 37, 809 (1976).

[8]U. R. Arifkhanov, N. A. Vlasov, V. V. Davydov, and L. N. Samoilov, J. Nucl. Phys. (U.S.S.R.) 2, 239 (1965).

[9]K. Imai, K. Hatanka, H. Shimizu, N. Tamura, K. Egawa, K. Nisimura, T. Saito, H. Sato, and Y. Wakuta, Nucl. Phys. A325, 397 (1979).

[10]F. N. Rad, R. G. Graves, D. P. Saylor, M. L. Evans, E. P. Chamberlin, J. W. Watson, and L. C. Northcliffe, Nucl. Instrum. Methods 190, 459 (1981).

[11]E. P. Chamberlin and R. A. Kenefick, Nucl. Instrum. Methods 190, 441 (1981).

[12]H. E. Conzett, W. Dahme, Ch. Leemann, J. A. Macdonald, and J. P. Meulders, in Proceedings of the Fourth International Symposium on Polarization Phenomena in Nuclear Reactions, edited by W. Grüebler and V. König (Birkhaüser, Basel, 1976), p. 566.

[13]J. E. Simmons, W. B. Broste, T. R. Donaghue, R. C. Haight, and J. C. Martin, Nucl. Instrum. Methods 106, 477 (1973).

[14]F. N. Rad, Ph.D. thesis, Texas A&M University, 1973, available from University Microfilms, Ann Arbor.

[15]J. E. Simmons, W. B. Broste, G. P. Lawrence, J. L. McKibben, and G. G. Ohlsen, Phys. Rev. Lett. 27, 113 (1971).

[16]L. C. Northcliffe, W. D. Cornelius, R. L. York, and J. C. Hiebert, in Polarization Phenomena in Nuclear Physics—1980 (Fifth International Symposium, Santa Fe), Proceedings of the Fifth International Symposium on Polarization Phenomena in Nuclear Physics, AIP Conf. Proc. No. 69, edited by G. G. Ohlsen, R. E. Brown, N. Jarmie, M. W. McNaughton, and G. M. Hale (AIP, New York, 1981), p. 1335.

[17]L. C. Northcliffe, W. D. Cornelius, J. C. Hiebert, and R. L. York (unpublished).

[18]R. L. York, W. D. Cornelius, L. C. Northcliffe, and J. C. Hiebert, see Ref. 16, p. 1461.

[19]C. M. Surko, R. E. Packard, G. J. Dick, and F. Reif, Phys. Rev. Lett. 24, 657 (1970).

[20]J. E. Simmons and R. B. Perkins, Rev. Sci. Instrum. 32, 1173 (1961).

[21]R. L. York, Ph.D. thesis, Texas A&M University, 1979, available from University Microfilms, Ann Arbor.

[22]F. N. Rad, L. C. Northcliffe, D. P. Saylor, J. G. Rogers, and R. G. Graves, Phys. Rev. C 8, 1248 (1973).

[23]R. G. Graves, M. Jain, H. D. Knox, E. P. Chamberlin, and L. C. Northcliffe, Phys. Rev. Lett. 35, 917 (1975).

[24]J. C. Hiebert, R. G. Graves, L. C. Northcliffe, R. L. York, E. P. Chamberlin, and J. M. Moss, Phys. Rev. Lett. 37, 276 (1976).

[25]S. T. Lam, D. A. Gedcke, G. M. Stinson, S. M. Tang, and J. T. Sample, Nucl. Instrum. Methods 62, 1 (1968).

[26]T. G. Miller, F. P. Gibson, and G. W. Morrison, Nucl. Instrum. Methods 80, 325 (1970).

[27]J. C. Hiebert (unpublished).

[28]P. R. Bevington, Data Reduction and Error Analysis for the Physical Sciences (McGraw-Hill, New York, 1969).

[29]S. Hayakawa, N. Horikawa, R. Kajikawa, K. Kikuchi, H. Kobayakawa, K. Matsuda, S. Nagata, and Y. Sumi, J. Phys. Soc. Jpn. 19, 2004 (1964).

[30]E. T. Boschitz, M. Chabre, H. E. Conzett, H. E. Shield, and R. J. Slobodrian, in Proceedings of the Fourth International Symposium on Polarization Phenomena in Nuclear Reactions, edited by W. Grüebler and V. König (Birkhaüser, Basel, 1976), p. 328.

[31]A. Houdayer, N. E. Davidson, S. A. Elbakr, A. M. Sourkes, W. T. H. van Oers, and A. D. Bacher, Phys. Rev. C 18, 1985 (1978).

[32]A. D. Bacher, G. R. Plattner, H. E. Conzett, D. J. Clark, H. Grunder, and W. F. Tivol, Phys. Rev. C 5, 1147 (1972).

[33]G. R. Plattner, A. D. Bacher, and H. E. Conzett, Phys. Rev. C 5, 1158 (1972).

[34]T. Saito, Nucl. Phys. A331, 477 (1979).

[35]J. H. Foote, O. Chamberlain, E. H. Rogers, and H. M. Steiner, Phys. Rev. 122, 959 (1961).

[36]M. K. Craddock, R. C. Hanna, L. P. Robertson, and B. N. Davies, Phys. Lett. 5, 335 (1963).

[37]J. Fröhlich, L. Streit, H. Zankel, and H. Zingl, J. Phys. G 6, 841 (1980).

[38]H. Zankel, see Ref. 16, p. 1413.

[39]J. Fröhlich, Z. Phys. A 302, 275 (1981).

[40]J. Fröhlich, H. Kriesche, L. Streit, and H. Zankel, Nucl. Phys. A384, 97 (1982).

[41]H. Zankel, private communication.

[42]H. O. Klages, private communication.